Meteorol Atmos Phys (2013) 122:33–45
DOI 10.1007/s00703-013-0269-1

ORIGINAL PAPER

An analysis of heavy precipitation caused by a retracing plateau vortex based on TRMM data

Shuoyu Xiang · Yueqing Li · Dian Li · Song Yang

Received: 17 March 2013 / Accepted: 29 May 2013 / Published online: 14 June 2013

Abstract In this paper, we study a persistent heavy precipitation process caused by a special retracing plateau vortex in the eastern Tibetan Plateau during 21–26 July 2010 using tropical rainfall measuring mission (TRMM) data. Results show that during the whole heavy rainfall process, the precipitation rate of convective cloud is steady for all four phases of the plateau vortex movement. Compared with the convective precipitation clouds, the stratiform precipitation clouds have a higher fraction of area, a comparable ratio of contribution to the total precipitation, and a much lower precipitation rate. Precipitation increases substantially after the vortex moves out of the Tibetan Plateau, and Sichuan Province has the most extensive precipitation, which occurs when the vortex turns back westward. A number of strong convective precipitation cloud centers appear at 3–5 km. With strong upward motion, the highest rain top can reach up to 15 km. In various phases of the vortex evolution, there is always more precipitable ice than precipitable water, cloud ice water and cloud liquid water. The precipitating cloud particles increase significantly in the middle and lower troposphere when the vortex moves eastward, and cloud ice particles increase quickly at 6–8 km when the vortex retraces westward. The center of the latent heat release is always prior to the center of the vortex, and the vortex moves along the latent heat release areas. Moreover, high latent heat is released at 5–8 km with maximum at 7 km. Also, the latent heat release is more significant when the vortex moves out of the Tibetan Plateau than over the Tibetan Plateau.

Responsible editor: M. Kaplan.

S. Xiang · Y. Li (✉)
China Meteorological Administration, Institute of Plateau Meteorology, Chengdu 610072, Sichuan, China
e-mail: yueqingli@163.com

D. Li
Shenyang Meteorological Office, Shenyang 110168, Liaoning, China

S. Yang
NOAA/Climate Prediction Center, College Park, MD 20740, USA

1 Introduction

In the eastern Tibetan Plateau and its surrounding areas, heavy precipitation often happens, largely because of the combined effects of complex multi-scale steep terrain and some special local weather systems. The plateau vortex is a unique weather system which often can cause rainfall and rainstorms. Typically, some plateau vortexes persist a long time with little movement, the other ones move out of the Tibetan Plateau along three paths (northeast, east or southeast) when there are favorable conditions, and it can bring severe weather over a broad region in China. For example, persistent rainstorm weather in the Yangtze River Valley in the summer of 1998 was caused by eastward moving plateau vortices (Zhang et al. 2002). Therefore, understanding the plateau vortex is crucial for predicting disastrous weather not only in and surrounding the Tibetan Plateau regions but also in the vast areas east of the Tibetan Plateau. However, due to lack of high temporal and spatial resolution data, the knowledge about the plateau vortex is limited, particularly for the physical mechanism, the associated precipitation evolution, the micro-physical characteristics, and the thermal structures.

Since the tropical rainfall measuring mission (TRMM) launched in 1997, the TRMM data have widely been used

to study tropical precipitation and climate (Tao et al. 1993; Schumacher et al. 2003; Short et al. 2000; Liu et al. 2008; Jiang et al. 2009; Wolff and Fisher 2009; Masunaga 2012). The TRMM satellite is known as "flying rain gauge" (Adler et al. 2000). In recent years, the TRMM data have also been used to study the weather and climate in the western China. Fu et al. (2007) used the TRMM precipitation radar (PR) measurements of summer 1998–2000 to analyze the climate characteristics of precipitation over the Tibetan Plateau. They found that the vertical distribution of plateau precipitation in the latitude and longitude directions is like a "tower". With TRMM PR and Global Precipitation Climatology Project data, Fu et al. (2008) studied the Tibetan Plateau precipitation and latent heating characteristics in summer, and re-defined the TRMM precipitation in the plateau as three types of deep strong convective, deep weak convective and shallow convective precipitation. They pointed out that the averaged latent heat over the plateau in summer was a single peak type, which differs from the bimodal peak type over the non-plateau area. Due to the large variations of the topography, and complex weather and climate systems on the eastern side of the Tibetan Plateau region, as well as the shortage of in situ observations (Yu et al. 2004; 2010; Li et al. 2010b), it is necessary to use the high spatial and temporal resolution TRMM data to reveal the dynamic and thermodynamics characteristics of heavy rainfall on the eastern side of the Tibetan Plateau region.

On July 21–26, 2010, a plateau vortex was observed, which moved out of the Tibetan Plateau at first, then turned back to the plateau. This vortex with the particular "retracing path" resulted in heavy rainfall on the eastern side of the Tibetan Plateau region and the surrounding areas. In this paper, mainly based on four orbit data from TRMM PR and TRMM Microwave Imager (TMI), we analyze precipitation structure, precipitation particle distribution and latent heat variations in different phases in the retracing path of this vortex evolution.

2 Weather background and data

During July 21–26 2010, a large range of heavy rainfall-related processes occurred on the eastern side of the Tibetan Plateau as it was affected by a plateau vortex. A northeast–southwest oriented strong rainfall belt developed from northern Sichuan and southern Shanxi with the heavy precipitation center in the northwestern Sichuan Basin. The total rainfall amount was >400 mm, the other precipitation centers were located in the adjoined region among Hubei, Henan, and Shanxi provinces, with precipitation amounts >200 mm (Fig. 1b). There was a favorable large-scale circulation for this convective precipitation process with a stable "two troughs and one ridge" pattern at 500 hPa (Fig. 1c, d). The two troughs were in Balkhash and in northeast China, respectively, and the high pressure and warm ridge in Lake Baikal at the Great Bend of Yellow River in China. The Mongolian high was belt-like and just was located to the west-north of the plateau vortex. And the subtropical high was developed and strong. The circulation pattern had an important influence on the movement of the plateau vortex (Fig. 1c, d). This was especially true because the subtropical high was stable expanding westward to the south of 35°N, and the Mongolian high strengthened and expanded eastward to the north of 35°N, the plateau vortex was forced to move along the retracing path, not along the normal paths such as northeastward, eastward and southeastward. Moreover, two southwesterly jets existed along 108°E at 700 hPa, and the maximum wind speed exceeded 20 m/s in their centers. This flow field brought much warm moist air to the climatologically favorable rainfall areas on the eastern side of the Tibetan Plateau (Figure not shown).

The moving plateau vortex is shown in Fig. 1a. At 08:00 on 21 July (Beijing Time, the same below), the plateau vortex formed over the eastern Tibetan Plateau. It gradually moved out of the Tibetan Plateau. On 21–23 July, the vortex continued to move eastward and affected northern Sichuan and southern Shanxi, which brought the persistent and strong rainfall (Fig. 1a, b). At 14:00 on 23 July, the Mongolian high strengthened to the north of the vortex (Fig. 1d), and the plateau vortex moved slowly eastward. At 14:00 on 24 July, the Mongolian high and the subtropical high were connected and formed a high pressure belt, and the plateau vortex gradually retraced toward the southwest, squeezed by the high pressure belt (Fig. 1a, d). On 25 July, the vortex continually moved southwestward and weakened, and precipitation gradually ended (Fig. 1a). Here, we need to emphasize that, compared to the rainstorm caused by a typical plateau vortex, this east-moving plateau vortex that suddenly turned to the west and produced heavy rainfall was rarely observed and investigated.

During the plateau vortex retracing process, the vorticity in the center at 500 hPa underwent significant changes in its strength (Fig. 2a). The vortex strengthened when it moved out of the plateau. When the vortex formed over the plateau, the average vorticity in the vortex area was about 4×10^{-5}/s. When the vortex moved out of the plateau, the vorticity at the vortex center increased rapidly to $>10 \times 10^{-5}$/s within 24 h. As the vortex retraced westward, the large values of the vorticity center persisted a while, then weakened quickly, with average vorticity $<4 \times 10^{-5}$/s.

In short, the vortex evolution shows that the vortex was triggered over the plateau and intensified when moving out of the plateau while later weakened rapidly when returning to the plateau. According to the evolution of divergence

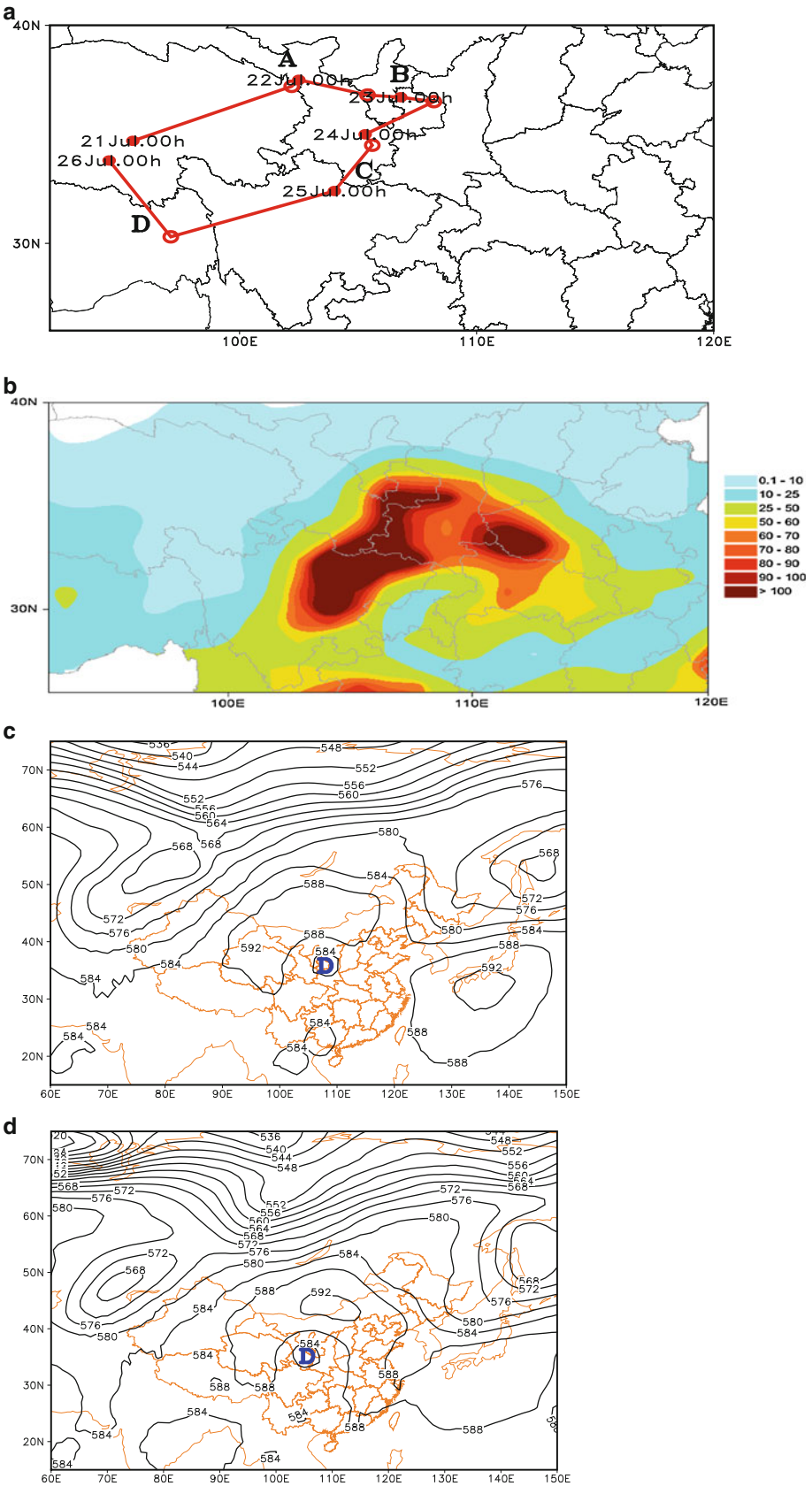

Fig. 1 **a** The path of movement of the plateau vortex during July 21–26, 2010. The *letters A*, *B*, *C* and *D* are at the time captured by TRMM in the phase A, B, C and D, respectively; **b** total precipitation caused by the plateau vortex during July 21–26, 2010; **c** geopotential height at 500 hPa at 14:00 July 23, 2010; **d** geopotential height at 500 hPa at 14:00 July 24, 2010. The *letter D* marks the position of the vortex. The time is Beijing time

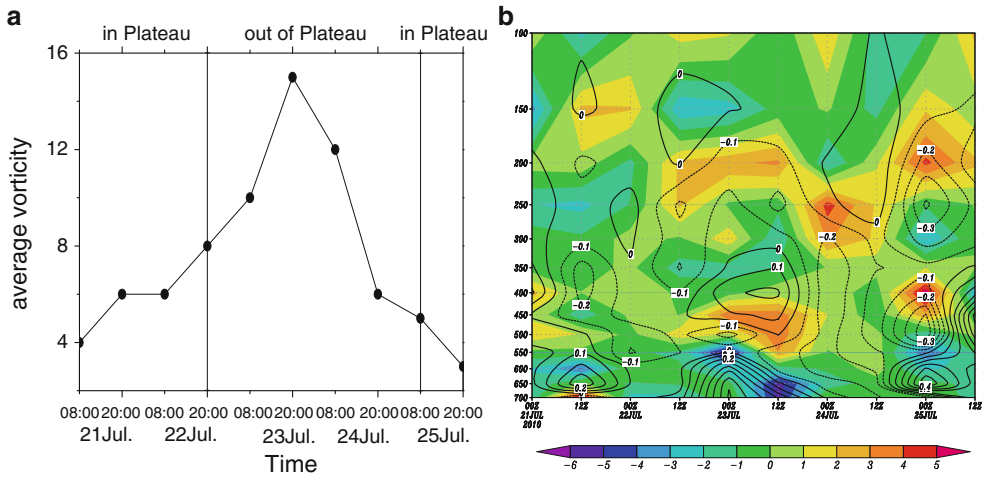

Fig. 2 **a** Time evolution of averaged vorticity of the plateau vortex at 500 hPa (unit: 10^{-5}/s) and **b** time-varying vertical cross-section of divergence (shading, unit: 10^{-5}/s) and vertical velocity (contour, units: Pa/s)

and vertical velocity at the vortex center (Fig. 2b), it is noted that the vortex center maintained a low-level convergence and upper-level divergence structure along the retracing path of the vortex. The convergence was very weak when the vortex was over the plateau, and enhanced significantly when the vortex moved out of the plateau. The vertical velocity at the vortex center was basically a subsidence flow below 550 hPa and ascending flow above 600 hPa, when the vortex was over the plateau. When the vortex moved out of the plateau, the ascending flow elevated to the tropopause. Subsidence near 400 hPa was observed on July 23, and the ascending flow was consistent in the vertical direction on July 24. The upward flow further enhanced within the upper-levels of the atmosphere on July 25, suggesting that an orographically induced flow was produced by the blocking effect of the Tibetan Plateau terrain when the vortex retraced westward.

The major data used in this work is from the TRMM project (Liu et al. 2012). To study tropical rainfall, the TRMM satellite was developed by NASA, USA, and NASDA, Japan, which successfully launched it on 27 November 1997. Its goal was to measure the tropical and subtropical precipitation and energy conversions (Olson et al. 2001; Liu et al. 2012). It has provided a large number of meteorological data, such as tropical ocean precipitation, cloud liquid water content, and latent heating rates. At present, the satellite height is about 402.5 km, covering the geographic range of 38°S–38°N and 180°W–180°E. The cycle is about 92.5 min a day, running about 16 tracks a day. There are five remote sensing instruments on TRMM, which are PR, TRMM microwave imager (TMI), visible and infrared scanner (VIRS), clouds and the earth's radiant energy sensor (CERES) and lighting imaging sensor (LIS) (Kawanishi et al. 1998; Kummerow et al. 1998; Liu et al. 2012). The data used in this manuscript include the standard products 2A25 and 2A12 provided by the TRMM data center (Kozu et al. 1998) organized separately by PR and TMI. 2A25 has a total of 80 layers of data, and it can measure the spatial distribution of precipitation from the ground to the altitude of 20 km. Its horizontal resolution is 4.5 km. 2A12 has five channels. In addition to the 21.3 GHZ channel are vertical mono-polarized channels: 10.7, 19.4, 37.0 and 85.5 GHZ, which are all dual-polarized channels (horizontal and vertical). The sounding height can be up to 18 km, and the horizontal resolution is 5.1 km in the 85.5 GHZ channel. Details about the data can be found in Kawanishi et al. (1998); Kummerow et al. (1998); Olson et al. (2001); Liu et al. (2012).

The TRMM satellite captured the strong convective precipitation process on the eastern side of Tibetan Plateau from 21–26 July 2010. We select four orbits of data corresponding to the vortex evolution: 23:35 21 July 2010 (denoted by Phase A), 01:55 23 July 2010 (denoted by Phase B), 22:26 24 July 2010 (denoted by Phase C), and 21:30 25 July 2010 (denoted by Phase D). The orbit numbers are 72,237, 72,254, 72,283 and 72,298. Phases A, B, C, and D correspond to the four moving phases of vortex evolution (see Fig. 1a): over the plateau (Phase A), moving eastward out of the plateau (Phase B), retracing westward (Phase C) and back to the plateau (Phase D). The corresponding regional precipitation evolution is: precipitation occurrence in Phase A, precipitation enhancement in Phase B, precipitation maximum in Phase C, and precipitation reduction in Phase D.

The other data which are used in this paper include: (1) the daily precipitation data of 1,700 meteorological stations in China were selected in the region inclusive of 92°–120°E and 26°–40°N during July 21–26, 2010, which are provided by National Meteorological Center, China. (2) United States National Centers for Environmental Prediction (NECP) FNL Operational Global Analysis data on

1.0° × 1.0° grids available four times a day from the Global Data Assimilation System (GDSA) and other sources of data surface pressure, sea level pressure, geopotential height, temperature, relative humidity, u- and v-winds, vertical motion, etc., parameters. We use geopotential height at 500 hPa during July 21–26, 2010 to analyze the circulation background of plateau vortex evolution over the region including 60°–150°E and 15°–75°N.

3 Precipitation structure

3.1 Horizontal structure

According to the precipitation inversion method of TRMM PR (Kummerow et al. 1998), the 2A25 precipitation data are classified into three types: convective (the echo of PR has no bright band and the echo intensity of radar is greater

Table 1 Statistics of convective and stratiform precipitation and their dependence on the phases of the plateau vortex evolution

Phase	Precipitation type	Area ratio (%)	Contribution to total precipitation amount (%)	Average precipitation rate (mm/h)
A	Convective (stratiform)	39 (61)	74 (26)	11.41 (1.82)
B	Convective (stratiform)	8 (92)	21 (79)	9.13 (2.03)
C	Convective (stratiform)	26 (74)	53 (47)	14.20 (2.97)
D	Convective (stratiform)	7 (93)	20 (80)	9.35 (1.94)

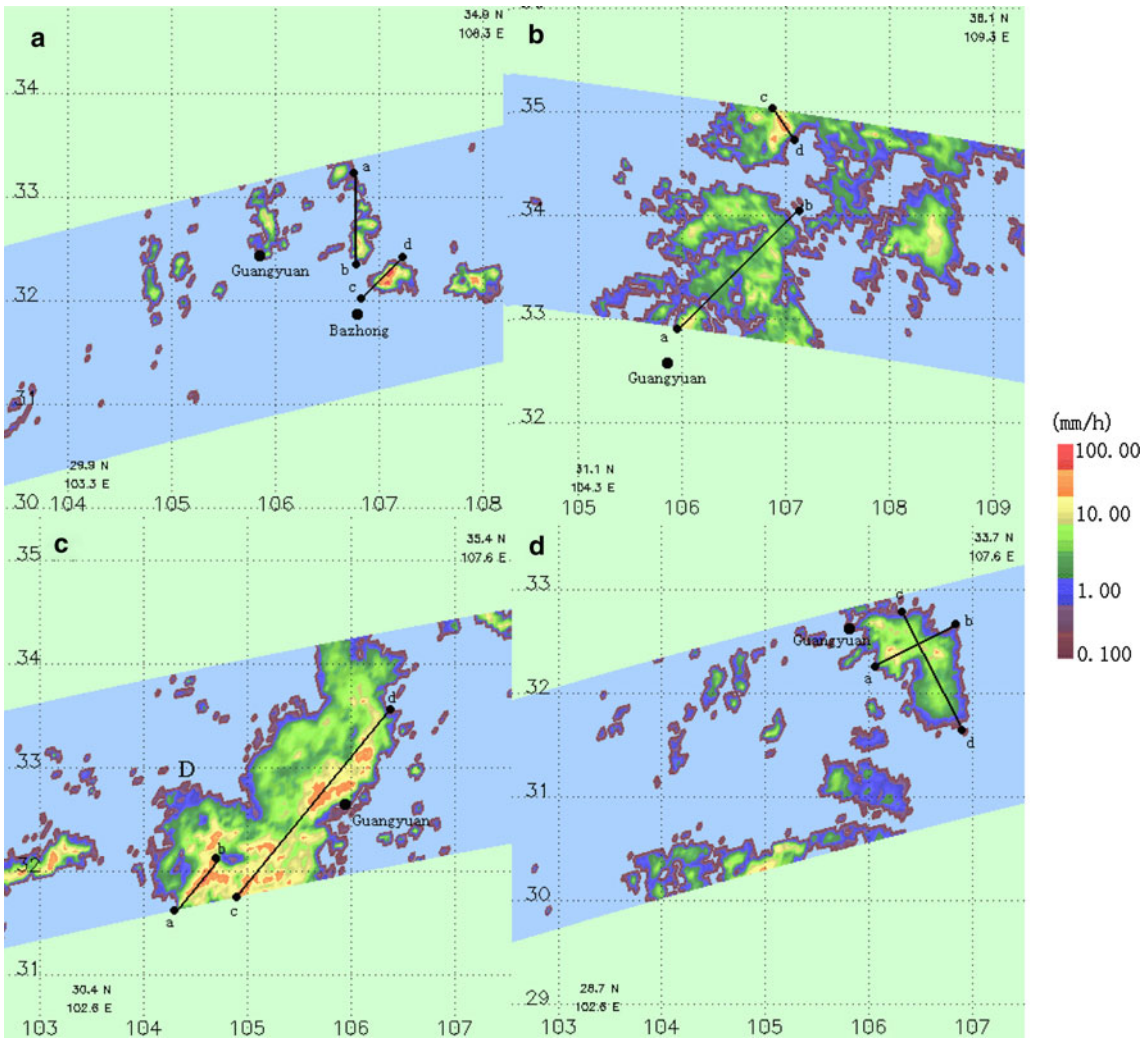

Fig. 3 Distribution of surface precipitation rate in the four phases of the plateau vortex movement: **a** over the plateau, **b** moving eastward out of the plateau, **c** retracing westward, and **d** back to the plateau. The *lines a–b* and *c–d* are the two vertical section positions of surface precipitation rate. The *letter D* marks the position of the vortex. (Units: mm/h)

than 39 dBz), stratiform (PR echo has a bright band near the freezing level) and the others (in addition to the two types of precipitation) (Awaka et al. 1998). According to this classification, we calculate the area fraction (grid points) of convective and stratiform precipitation clouds, ratio of different type of precipitation to total precipitation, and the average precipitation rate of different type precipitations in the different phases of the vortex evolution (Table 1).

From Table 1, we note that the area fraction of convective precipitation is in a range of 7–39 % for four phases. The area fraction also changes with its phase. It is large in Phase A, decreases from Phase A to B, then increases from Phase B to C, and decreases again in Phase D. The contribution ratio of the convective precipitation contribution to total precipitation amount is in a range of 20–74 %. Moreover, the areal fraction of stratiform precipitation clouds is almost linearly related to the ratio of its contribution to total precipitation amount. Approximately, the ratio of the contribution of convective cloud to total precipitation amount is 2–3 times of the areal fraction of convective cloud, suggesting convective precipitation covers a smaller area with a larger contribution to total precipitation amount, compared with the stratiform cloud. The precipitation rate is steady for precipitation for all four phases in a range of 9.13–14.20 mm/h.

Compared with the convective precipitation, on average, stratiform precipitation has a higher areal fraction in a range of 61–93 %, comparable ratio of contribution to the total precipitation amount in a range of 26–80 %, and much lower precipitation rate in a range of 1.82–2.97 mm/h (Table 1). This suggests that stratiform precipitation

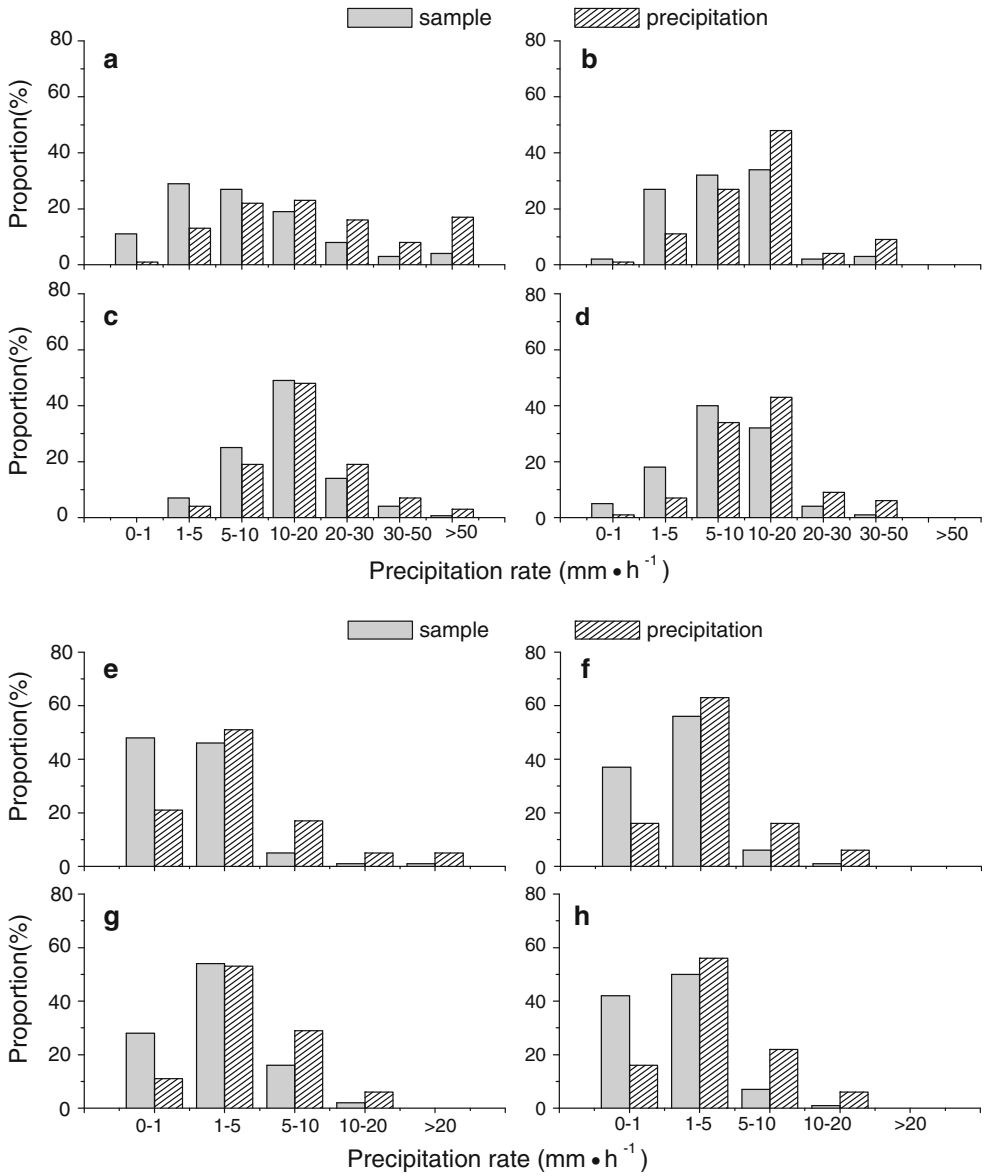

Fig. 4 Relationship of surface precipitable water and frequency for convection (**a**–**d**) and stratiform (**e**–**h**) clouds in the four phases of the plateau vortex movement

associated with the vortex has larger spatial scale, lower precipitation rate with longer persistency, and comparable precipitation amount, compared with that of the convective precipitation. Also, different phases have different ratios of the two types of precipitation. For example, precipitation is dominated by convective precipitation in Phase A, by stratiform precipitation in Phases B and D, and the contribution is almost equivalent from the convective and stratiform precipitation in Phase C.

These results indicate that the vortex is accompanied largely by convective precipitation when it was over the plateau (Phase A) and by stratiform precipitation when it moved eastward out of the plateau or returned back to the plateau (Phases B and D). The convective and stratiform precipitations contribute almost equal when the vortex retraced westward (Phase C). These results are consistent with Fu et al. (2003). By analyzing two strong meso-scale convective systems in Wuhan and southern Anhui, they suggested that the average precipitation rate is related to the precipitation types. Nevertheless, the horizontal structures of precipitating clouds they studied are different from this work. For instance, the meso-scale convective systems in Wuhan and southern Anhui generate a number of strong rain cells and large rain belts, while the processes associated with the plateau vortex mainly generates a strong rain band.

The horizontal distribution of near-surface precipitation in the four phases of plateau vortex evolution is shown in Fig. 3. It is noted that the precipitation system is composed of scattered cloud cells in Phase A. The precipitation rate in northern Sichuan is about 131 mm/h. In Phase B, the clouds expand and gradually develop into a meso-α scale

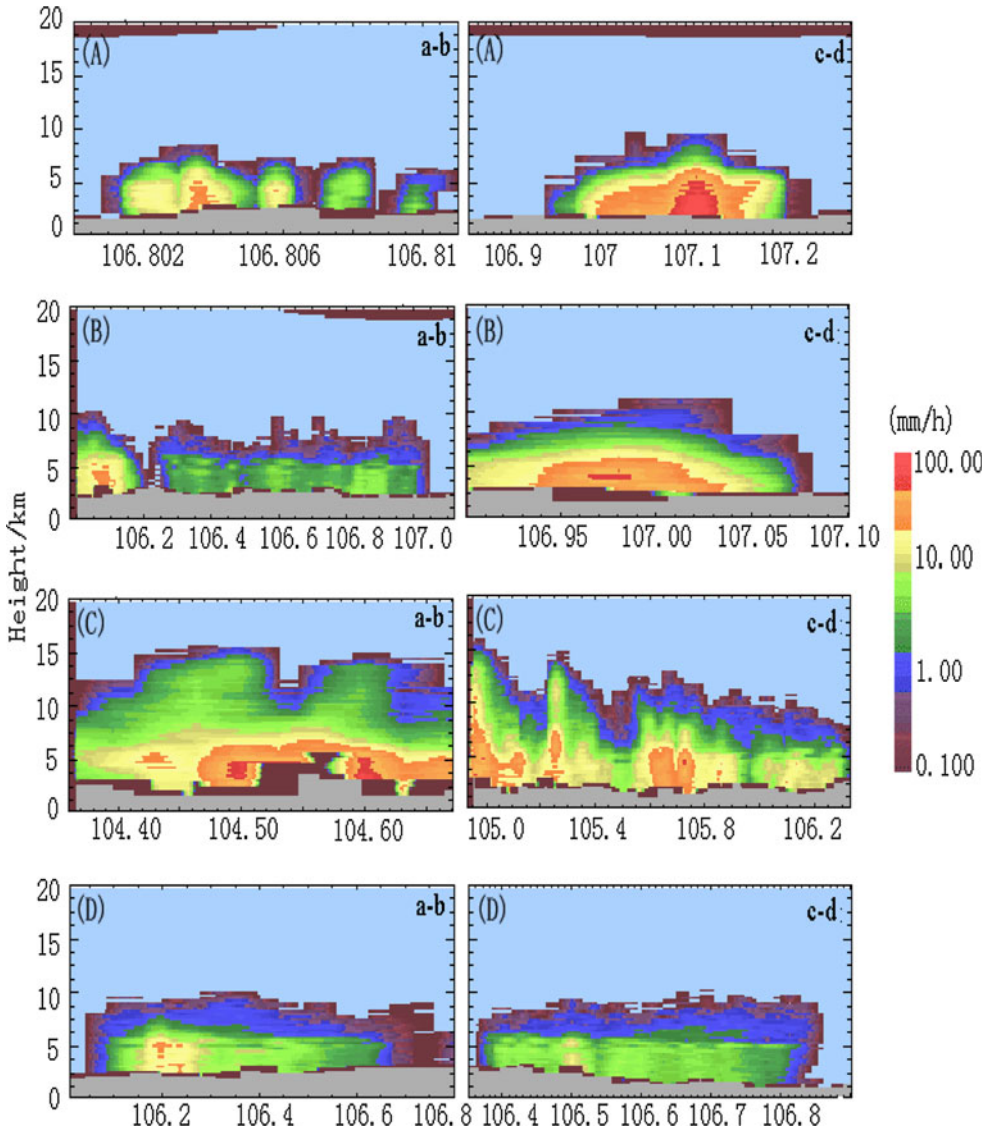

Fig. 5 Vertical section of precipitating clouds in the four phases of the plateau vortex movement. **A** Over the plateau, **B** moving eastward out of the plateau, **C** retracing westward, and **D** back to the plateau. In the *top right* corner of (**A**), (**B**), (**C**) and (**D**), the *a–b* (*left*) and *c–d* (*right*) denote the two vertical section positions in Fig. 3. (Units: mm/h)

system. The precipitation is insignificant at about 10 mm/h, and the rainfall area enlarges. In Phase C, the plateau vortex moves to the northwest of Sichuan Province, and the precipitating clouds further develop as a main precipitating cloud cluster and some scattered precipitating clouds. Meanwhile, several heavy precipitation and strong convective centers appear in northern Sichuan. In Phase D, the heavy precipitation centers disappear, and the precipitation system is separated into scattered weak precipitating clouds.

It is known that the characteristics of the precipitation spectrum can reflect the cloud features. An analysis on the precipitation spectrum of the two types of precipitating clouds (convective and stratiform) (Fig. 4) shows that the spectrum is wider for convective precipitation than for stratiform precipitation during the entire plateau vortex evolution. The percentage of higher rainfall intensity (>30 mm/h) first decreases, then increases, and later decreases again, following the convective weather change. This is also consistent with the above analysis based on Table 1.

3.2 Vertical structure

Figure 5 is the vertical section of precipitating cloud along the lines a–b, c–d (shown in Fig. 3) in the four Phases of the vortex evolution. In Phase A, the cloud top is lower than 10 km. According to line c–d, the "tower" structure of the convective cloud is weak, the largest cloud center is in 3–5 km height, and the maximum precipitation rate is >100 mm/h. In Phase B, the height of 10 mm/h precipitation remains at 6 km, and the strongest precipitation center is at 4 km. In Phase C, the precipitating cloud further develops and reaches to a higher level, where the maximum height is over 15 km. The height of maximum precipitation top is distributed irregularly. In Phase D, the overall precipitating cloud top height drops to below 10 km, and there is a bright band of 0 °C at 5 km in line c–d. It indicates that the convective cloud changes into stratiform cloud.

The precipitating cloud top height is the highest layer of precipitation rate observed by TRMM PR, measuring the characteristics of precipitating clouds in the vertical direction. Analyzing the precipitating cloud top height of each grid point and its relation with the near-surface precipitation in the different phase of the vortex evolution (Fig. 6), it is found that the top is much higher when the vortex moved out of the plateau (Fig. 6c) than the vortex over the plateau (Fig. 6a, d). The precipitating cloud top significantly increases when the vortex retraced westward, and the highest precipitating cloud top is >15 km (Fig. 6c). Meanwhile, the highest precipitating cloud tops are all around 10 km with smaller variability in the other phases. Also, in every phase, on average, the precipitating cloud top increases with increasing near-surface precipitation. Averaged precipitable profiles are shown in Fig. 7. Considering the topography in northern Sichuan, we analyze the convective and stratiform average precipitating cloud profiles over 3 km height in the four phases of the plateau vortex evolution. The result shows that the variability of the stratiform cloud profiles in all phases is smaller than that of the

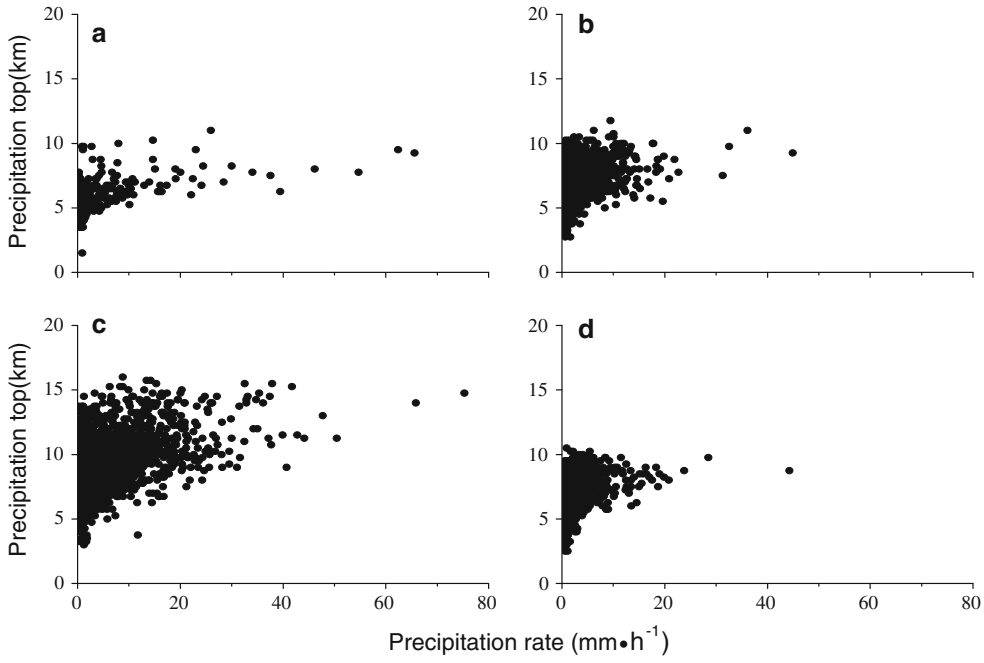

Fig. 6 The top height of the convective clouds compared with near-surface precipitation in the four phases of the plateau vortex movement

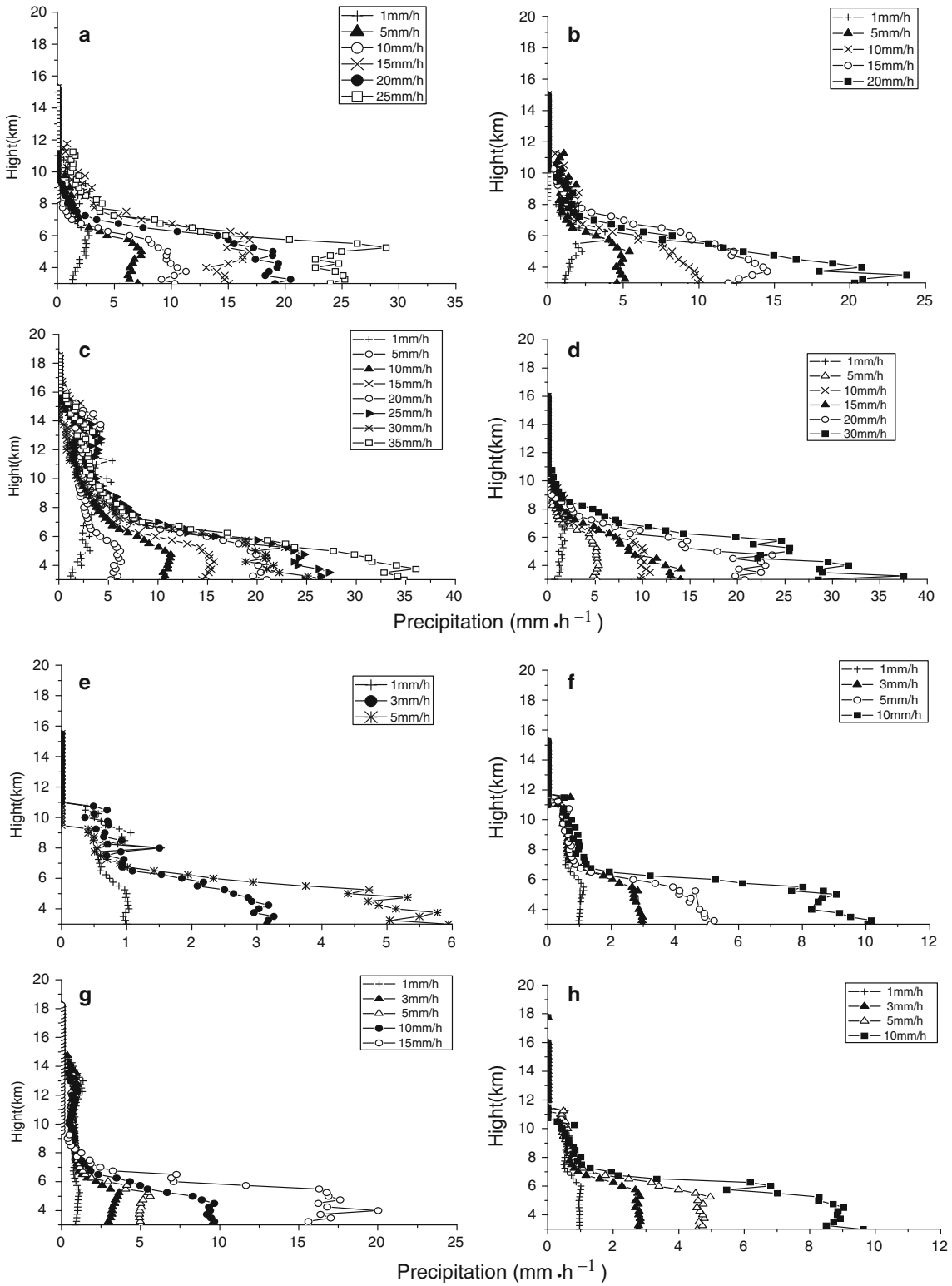

Fig. 7 Average precipitating cloud profiles above 3 km of the convection (**a**–**d**) and stratiform (**e**–**h**) in the four phases of the plateau vortex movement

convective cloud profiles, consistent with the fact that stratiform precipitation is more stable than convective precipitation.

Figure 8 shows the total content of four types of precipitation particles (precipitable ice, precipitable water, cloud ice water and cloud liquid water) in each layer in the

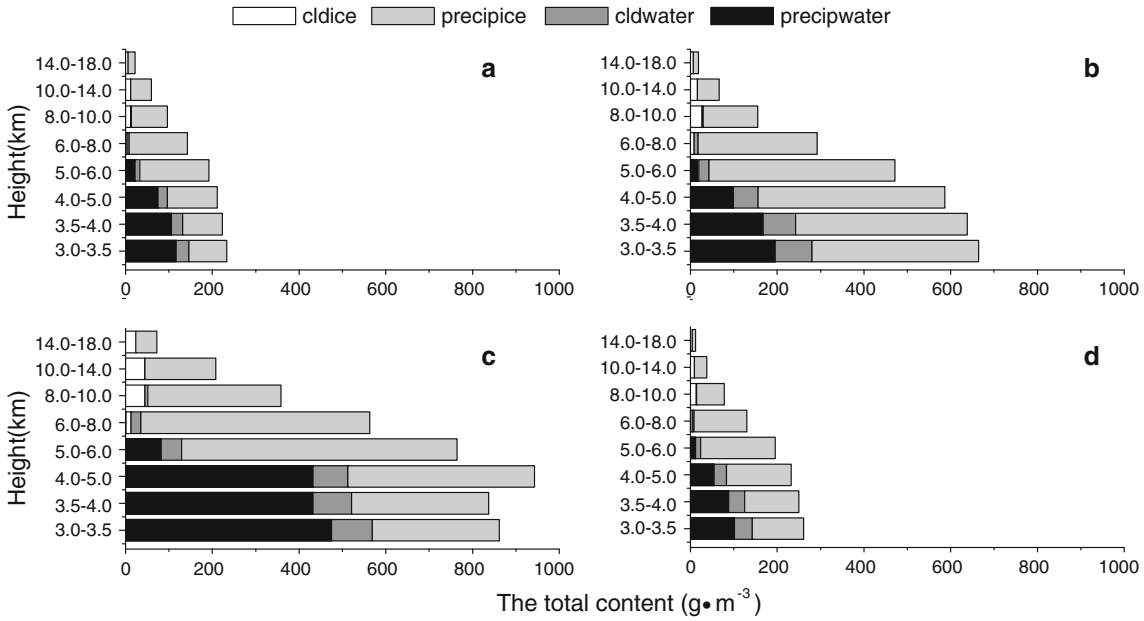

Fig. 8 Total content of precipitation particles (precipitable ice, precipitable water, cloud ice water and cloud liquid water) varied with height in the four phases of the plateau vortex movement

four phases of the vortex evolution sounding by TRMM. It is noted that the content of precipitable ice particles is always the highest in the four phases, the precipitable water particles is second, the cloud liquid water particles is third, and the cloud ice particles is the lowest amount. The precipitable ice particles appear mainly around 5–6 km, precipitable water particles and cloud liquid water particles mainly concentrate below 5 km, and cloud ice particles are mainly present in the high level.

The vertical distribution of precipitable water particles is coupled to the vertical distribution of the latent heat release, which is mainly released by the condensation process due to the conversion of water vapor to liquid particles. In the phase of the vortex movement out of the plateau (Fig. 8b), with the expansion of precipitation area, the content of each of the four types of precipitation particles increases in each layer, and the increase rate of precipitable ice particles above 6 km is less than that below 6 km, showing the precipitable water mainly in the mid-low level. In the phase of the vortex retracing westward (Fig. 8c), the content of precipitable ice particles continuously increases above 5 km, but decreases below 5 km. Meanwhile, the content of precipitable water particles increases significantly below 5 km, and the corresponding latent heat release is the strongest. The content of cloud ice particles increases substantially in the middle-upper troposphere (6–18 km), indicating that a large number of precipitable water particles form into solid shapes because of ascending into a high layer. In the phase of the vortex back to the plateau (Fig. 8d), the four types of the particles are reduced substantially in all layers, and the precipitation declines in a consistent manner.

The plateau vortex development and movement are also connected with the thermal structure of the vortex. When the vortex moved eastward out of the plateau, the center of latent heat release is located to the southeast of the vortex (Fig. 9a). When the vortex retraced to the plateau, the center of latent heat release is located to the southwest of the vortex (Fig. 9b, c). That suggests the latent heat release center is always preceding the vortex center, and the vortex develops and moves along the high-value areas of latent heat release.

The total latent heat released in each layer above 3 km in different phases is shown in Fig. 10. Large latent release is mainly around 5–8 km with the maximum value at 7 km. In the phases of the vortex moving eastward and retracing westward, the latent heat release increases rapidly to the first peak value, and then decreases rapidly in the 7–9 km layer. In the 9–14 km layer, the latent heat release increases a little and then declines again, while in the 14–16 km layer, the latent heat release increases once more.

These changes are related to the phase transition process in the precipitable water clouds. When the vortex is over the plateau, the total latent heat release in each layer indicates little difference, but it still shows a "two peak" structure. These results are similar to Li et al. (2009; 2010a). They noted the "two peak" structure and the

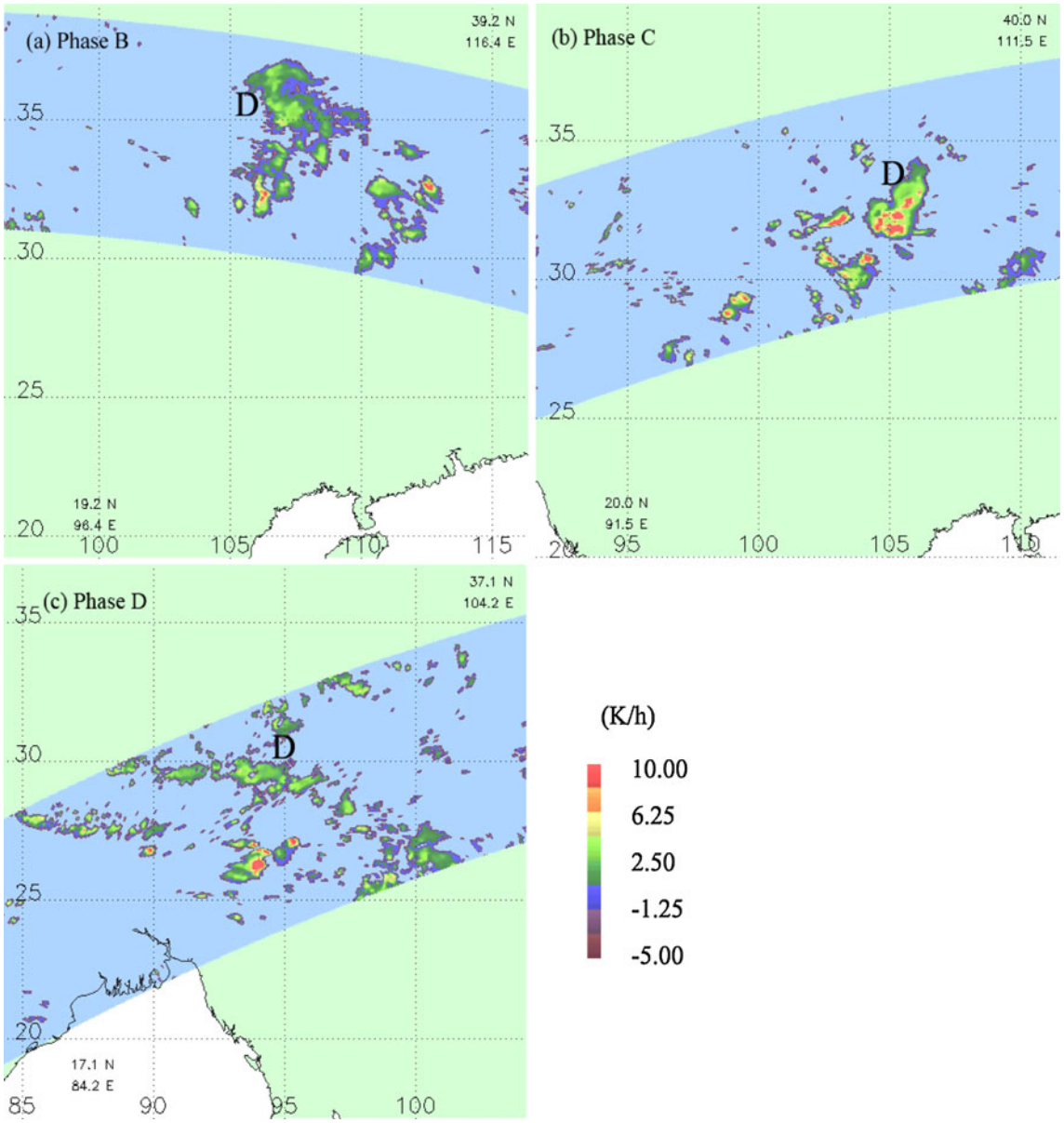

Fig. 9 Horizontal distribution of latent heat release at 7 km height in **a** during phase B: moving eastward out of the plateau, **b** during phase C: retracing westward and **c** during phase D: back to the plateau during the plateau vortex movement. The *letter D* marks the position of the vortex (Units: k/h)

largest latent heat released at 7 km during an excessive rainfall event in southern Sichuan. But these results are different from the "single peak" structure in Qinghai-Tibet Plateau analyzed by Liu et al. (2007). That may imply that the vertical structure of latent heat release depends on the precipitation system, location and phase.

4 Conclusions

In this work, we analyze a strong precipitation process caused by a plateau vortex on the eastern side of the Tibetan Plateau and the surrounding areas during July 21–26 July, 2010. The large-scale circulation pattern observed includes "two troughs and one ridge" in middle-high latitudes, a persistent eastward extended Mongolian high, and westward extended subtropical Pacific high. A long-lasted meso-scale vortex at 500 hPa is an important factor in promoting the development of heavy rainfall weather, especially when the vortex moved eastward out of the plateau first, then suddenly retraced back to the plateau, which directly causes this long persistent rainstorm process. Based on TRMM satellite data, we examine the horizontal and vertical structure, the characteristics of

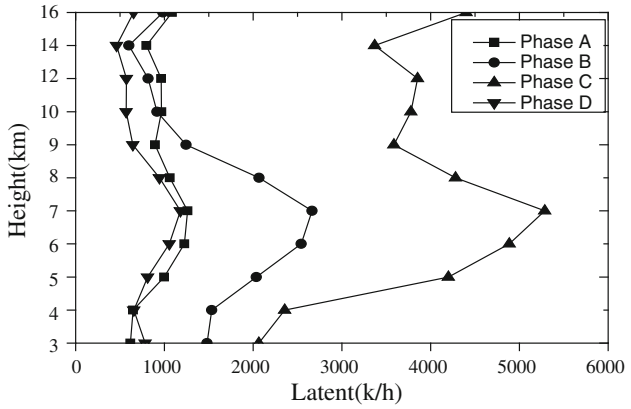

Fig. 10 Total latent heat release varied with height in the four phases of the plateau vortex movement

precipitating cloud profiles, the top height of precipitating clouds, the latent heat release profiles and the content of precipitation particles in the four phases of the vortex evolution. The main results are as follows:

1. The convective clouds are weak with scattered cloud cells when the vortex was over the plateau, and then strengthens when the vortex moved out of the plateau. When the vortex turned back westward to the plateau, both precipitation area and amount reach their maximum. It is noted that the fraction of stratiform cloud area is almost linearly correlated to the ratio of its contribution to total precipitation amount. Approximately, the ratio of contribution of convective cloud to total precipitation is 2–3 times of the areal fraction of convective cloud, suggesting a smaller area having convective precipitation and the contribution to total precipitation amount being larger. The precipitation rate for convective precipitation is in a range of 9.13–14.20 mm/h for all four phases. Compared with the convective precipitation, stratiform precipitation contributes a comparable ratio to the total precipitation amount although it has a higher fraction of area but a much lower precipitation rate. This suggests that stratiform precipitation associated with the vortex has larger spatial scale, lower precipitation rate with longer persistency, and comparable precipitation contribution, compared with that of the convective precipitation.
2. The cloud top is much higher when the vortex moved out of the plateau than the vortex over the plateau. The top height significantly increases to >15 km when the vortex retraced westward. Meanwhile, during the highest rainfall rate the cloud top is around 10 km with smaller variability in the other phases. In every phase, on average, the cloud top height increases with increase in near-surface precipitation. Furthermore, the variability of the stratiform cloud profiles in all four phases are smaller than that of the convective cloud profiles, consistent with the fact that stratiform precipitation is more stable than convective precipitation.
3. In the four phases, the content of precipitable ice particles is always largest, the precipitable water particles is second, the cloud liquid water particles is third, and the cloud ice particles is the lowest. The precipitable ice particles appear mainly around 5–6 km, precipitable water particles and cloud liquid water particles mainly concentrate below 5 km, and cloud ice particles are mainly present in the high level. Also, the contents of four types of precipitation particles depend on the phase of vortex evolution.
4. It is suggested that the latent heat release center is always preceding the vortex center and the vortex develops and moves to the high-value areas of latent heat release. In the all phases, large latent release is mainly centered around 5–8 km with the maximum value at 7 km and then decreases rapidly in the 7–9 km layer. The latent heat increases a little, and then declines in the 9–14 km layer again, while in 14–16 km, the latent heat release increases once more. Furthermore, in the phases of eastward movement and westward retracement of the plateau vortex, the latent heat release increases rapidly to the high value much greater than it in the other two phases.

In addition, the combined effects of the subtropical high and the Mongolian high mainly result in the retracing path of the plateau vortex movement. The general circulation pattern and interaction between different systems are the important reason for the abnormal movement of plateau vortex. And the strong moisture transfer from the low latitude is a key condition for the persistent heavy precipitation.

Acknowledgments The authors are grateful to Dr. Michael L. Kaplan who helped to improve the English and edit the manuscript. This work was supported by the National Key Basic Research Development Program Project of China (No. 2012CB417202), the National Natural Science Foundation of China (No. 41275051), Special Fund for Meteorological Research in the Public Interest (GYHY201206042, GYHY201106003, GYHY201006053), Special Research Funds Project of National Public Service Sectors (WMO), Key Research and Operation Project of Southwest China Regional Meteorological Center (No. 2010-1); Special Project for Basic Work of Ministry of Science and Technology (No. 2006FY220300).

References

Adler RF, Huffman GJ, Bolvin DT, Curtis S, Nelkin EJ (2000) Tropical rainfall distributions determined using TRMM combined with other satellite and rain gauge information. J Appl Meteor 39(12):2007–2023

Awaka J, Iguchi T, Okamoto K (1998) Early results on rain type classification by the Tropical Rainfall Measuring Mission (TRMM) precipitation radar. Proceedings of 8th URSI Commission F Open Symp, Aveiro, Portugal, pp 143–146

Fu YF, Yu RC, Xu YP, Xiao QN, Liu GS (2003) Analysis on precipitation structures of two heavy rain cases by using TRMM PR and TMI. Acta Meteor Sinica 61(4):421–431 (in Chinese)

Fu YF, Li HT, Zi Y (2007) Case study of precipitation cloud structure viewed by TRMM satellite in a valley of the Tibetan Plateau. Plateau Meteorol 26(1):98–106 (in Chinese)

Fu YF, Liu Q, Zi Y, Feng S, Li YQ, Liu GS (2008) Summer precipitation and latent heating over the Tibetan Plateau based on TRMM measurements. Plateau Mt Meteor Res 28(1):8–18 (in Chinese)

Jiang XN, Waliser DE, Olson WS, Tao WK, L'Ecyer TS, Li JL, Tian BJ, Yung YL, Tompkins AM, Lang SE, Grecu M (2009) Vertical heating structures associated with the MJO as characterized by TRMM estimates, ECMWF reanalyses, and forecasts: a case study during 1998/99 winter. J Clim 22(22):6001–6020

Kawanishi T, Kuroiwa H, Ishido Y, Umehara T, Kozu T, Okamoto K (1998) On-orbit test and calibration results of TRMM precipitation radar. Proceedings of SPIE on Microwave Remote Sensing of the Atmosphere and Environment Beijing China, pp 94–101

Kozu T, Lguchi T, Meneghini R, Awaka J, Okamoto K (1998) Preliminary test results of a rain rate profiling algorithm for the TRMM precipitation radar. Proceedings of SPIE on Microwave Remote Sensing of the Atmosphere and Environment, Beijing China, pp 86–93

Kummerow C, Barnes W, Kozu T, Shiue J, Simpson J (1998) The tropical rainfall measuring mission (TRMM) sensor package. J Atmos Oceanic Technol 15(3):809–817

Li DJ, Li YQ, Liu C, Gu QY (2009) Study on the "07.7.9" mesoscale torrential rain in south Sichuan based on TRMM observations. Torrential Rain Disasters 28(3):235–240 (in Chinese)

Li DJ, Li YQ, Liu C, Lin L (2010a) Comparative analysis between two summer heavy rain events in Yibin based on the TRMM data. Acta Meteor Sinica 68(4):559–568 (in Chinese)

Li YQ, Li DJ, Yang S, Liu C, Zhong AH, Li Y (2010b) Characteristics of the precipitation over the eastern edge of the Tibetan Plateau. Meteor Atmos Phys 106(1–2):49–56

Liu Q, Fu YF (2007) Characteristics of latent heating over the Tibetan Plateau during summer. J Univ Sci Technol China 37(3):303–309 (in Chinese)

Liu CT, Zipser EJ, Cecil DJ, Nesbitt SW, Sherwood S (2008) A cloud and precipitation feature database from nine years of TRMM observation. J Appl Meteor Climatol 47(10):2712–2728

Liu Z, Ostrenga D, Teng W, Kempler S (2012) Tropical rainfall measuring mission (TRMM) Precipitation data and services for research and applications. Bull Amer Meteor Soc 93(9):1317–1325

Masunaga H (2012) A satellite study of the atmospheric forcing and response to moist convection over tropical and subtropical oceans. J Atmos Sci 69(1):150–167

Olson WS, Bauer P, Viltard NC, DE Johnson, Tao WK, Meneghini R, Liao L (2001) A melting-layer model for passive/active microwave remote sensing applications. Part I: model formulation and comparison with observations. J Appl Meteor 40(7):1145–1163

Schumacher C, Houze RA (2003) Stratiform rain in the tropics as seen by the TRMM precipitation radar. J Clim 16(11):1739–1756

Short DA, Nakamura K (2000) TRMM radar observations of shallow precipitation over the tropical oceans. J Clim 13(23):4107–4124

Tao WK, Lang S, Simpson J, Adler R (1993) Retrieval algorithms for estimating the vertical profiles of latent heat release: their applications for TRMM. J Meteor Soc Japan 71(6):685–700

Wolff DB, Fisher BL (2009) Assessing the relative performance of microwave-based satellite rain-rate retrievals using TRMM ground validation data. J Appl Meteor Climato 48(6):1069–1099

Yu RC, Wang B, Zhou TJ (2004) Climate effects of the deep continental stratus clouds generated by the Tibetan Plateau. J Clim 17(13):2702–2713

Yu RC, Yuan WH, Li J, Fu YF (2010) Diurnal phase of late-night against late-afternoon of stratiform and convective precipitation in summer southern contiguous China. Clim Dyn 35(4):567–576

Zhang S, Tao S (2002) The influences of the Tibetan Plateau on weather anomalies over Yangtze River in 1998. Acta Meteor Sinica 60(4):442–452 (in Chinese)